Journal of Power Sources 195 (2010) 3402–3406

Contents lists available at ScienceDirect

Journal of Power Sources

journal homepage: www.elsevier.com/locate/jpowsour

Enhanced ionic transport in fine-grained scandia-stabilized zirconia ceramics

Paula M. Abdala[a], Graciela S. Custo[b], Diego G. Lamas[a,*]

[a] CINSO (Centro de Investigaciones en Sólidos), CONICET-CITEFA, J.B. de La Salle 4397, (B1603ALO) Villa Martelli, Pcia. de Buenos Aires, Argentina
[b] Gerencia de Área Seguridad Nuclear y Ambiente, Gerencia Química, Departamento Química Analítica, Centro Atómico Constituyentes, Comisión Nacional de Energía Atómica, Av. Constituyentes 1499, (B1650KNA) San Martín, Pcia. de Buenos Aires, Argentina

ARTICLE INFO

Article history:
Received 16 November 2009
Received in revised form 7 December 2009
Accepted 8 December 2009
Available online 16 December 2009

Keywords:
ZrO_2–Sc_2O_3
Ceramics
Electrical properties
Grain-boundary diffusion

ABSTRACT

In this work, the transport properties of fine-grained scandia-stabilized zirconia ceramics with low Si content have been investigated. These materials were prepared from ZrO_2–6 mol% Sc_2O_3 nanopowders synthesized by a nitrate-lysine gel-combustion route. High relative densities and excellent electrical properties were obtained, even for sintering temperatures as low as 1350 °C. Our electrochemical impedance spectroscopy study showed that both the volume fraction of grain boundaries and the specific grain-boundary conductivity are significantly enhanced with decreasing grain size, resulting in a higher total ionic conductivity.

1. Introduction

In recent years, the transport properties of nanostructured or fine-grained oxide-ion solid electrolytes have been intensively investigated. Even though several authors reported an increase in the total ionic conductivity in these materials [1–7], mainly attributable to their 'parallel' grain-boundary conductivity, there is great controversy regarding this subject.

In microcrystalline solid electrolytes, it is well known that grain boundaries partially block ionic transport, causing an extra contribution to the total resistance and, therefore, the total conductivity decreases with decreasing grain size. Remarkably, in ZrO_2- and CeO_2-based ceramics, it has been found that the specific, or 'true', grain-boundary conductivity (normalized by the volume fraction of the grain boundary: $\sigma'_{gb} = \sigma_{gb}\delta/D$, where σ_{gb} is the usual total grain-boundary conductivity, δ is the thickness of the grain boundary and D is the grain size) is orders of magnitude lower than that of the bulk, even in high-purity samples, indicating that this is an intrinsic property of the grain boundaries in these fluorite-like oxides [8–10]. Then, ionic transport across grain boundaries parallel to the current direction ('parallel' grain-boundary conductivity) can be ignored, not only because of the small volume fraction of grain boundaries, but also because of their relatively low diffusivity.

Contrarily, in nanostructured solid electrolytes, or even in some fine-grained materials, the volume fraction of grain boundaries is much larger and also the specific grain-boundary conductivity may increase [1]. In this case, the effect of the parallel grain-boundary transport may give rise to an increase in the total ionic conductivity, which may become higher than the bulk conductivity. However, only a few authors have observed this effect. For example, Kosacki and co-workers reported an increase by one or two orders of magnitude in the total ionic conductivity of nanostructured CeO_2–Gd_2O_3 and yttria-stabilized zirconia (YSZ) thin films, compared to that of polycrystals with a larger grain size [11,12]. A similar phenomenon has been found by our research group in ceria-based nanoceramics [6,7], which was attributed to the increase in the parallel grain-boundary conductivity of the nanostructured samples, coupled to an increase in the grain-boundary ionic diffusivity with decreasing grain size. Finally, Monty and co-workers found a similar effect in ZrO_2–4 mol% Y_2O_3 nanoceramics [2,3]. However, other authors did not observe this effect [13,14].

Scandia-stabilized zirconia (ScSZ) electrolytes exhibit excellent ionic conductivity, the highest among all ZrO_2-based materials [15]. For this reason, ScSC ceramics are considered as promising candidates for solid electrolytes in intermediate-temperature solid oxide fuel cells (IT-SOFCs) and other electrochemical devices. The optimum ionic conductivity corresponds to Sc_2O_3 contents between 9 and 11 mol%. Unfortunately, a rhombohedral phase (known as the β-phase) of poor electrical properties, which has not been observed in other ZrO_2-based materials, exists at low-temperatures for this compositional range [16]. The β-phase transforms to the high-conductivity cubic phase on heating at temperatures above 600 °C, reverting to the β-phase on cooling at about 500 °C. This $\beta \Leftrightarrow$ cubic phase transformation is undesirable for applications because it

* Corresponding author. Tel.: +54 11 47098100/1145; fax: +54 11 47098158.
E-mail address: dlamas@citefa.gov.ar (D.G. Lamas).

0378-7753/$ – see front matter © 2009 Elsevier B.V. All rights reserved.
doi:10.1016/j.jpowsour.2009.12.035

involves a volume change that can cause the deterioration of the electrolyte. Therefore, from a technological point of view, it is important to avoid this transformation without a dramatic loss in the ionic conductivity. For this purpose, the introduction of co-dopants that promote the retention of the cubic phase, such as Y_2O_3 or CeO_2, has been proposed [17–20]. On the other hand, some authors demonstrated that the β-phase can be avoided in fine-grained ScSZ ceramics, without the introduction of other dopants [21,22]. In fact, our research group has recently shown that the β-phase is absent in nanocrystalline ZrO_2–Sc_2O_3 solid solutions and we have proposed a phase diagram for materials with average crystallite sizes of about 25 nm [23].

Despite the importance of ScSZ solid electrolytes in SOFC technology, little information regarding the transport properties of nanostructured or fine-grained ScSZ ceramics can be found in the literature. Lei and Zhu reported the preparation of dense ScSZ ceramics with an average grain size of about 80 nm [21], but these authors only evaluated the total ionic conductivity, which was found to decrease with decreasing grain size, and grain-boundary transport was not investigated. Other authors analyzed ScSZ nanoceramics prepared by spark plasma sintering [22,24], but these materials exhibited low relative densities, so their results could be affected by the poor contact between grains. Finally, Xu et al. investigated the ionic transport properties of fine-grained ScSZ ceramics prepared from nanopowders synthesized by a mild urea-based hydrothermal method [25]. Interestingly, these authors found that the specific grain-boundary conductivity increases with decreasing average grain size but the total ionic conductivity remains lower than the bulk one.

The enhancement of the specific grain-boundary conductivity with decreasing grain size has also been found in other ZrO_2-based materials, such as ZrO_2-CaO and ZrO_2–Y_2O_3 [8,10,26,27]. Particularly, in the case of ZrO_2–CaO ceramics, Aoki et al. investigated the effect of impurities and proposed that the specific grain-boundary conductivity decreases with increasing grain size due to grain size-dependent segregation of Si and Ca [8]. However, these authors found that the specific grain-boundary conductivity is about two orders of magnitude lower than the bulk conductivity in high-purity samples. This fact indicates the existence of an intrinsic "blocking" effect which cannot be attributed to impurities. This intrinsic behavior of grain boundaries has been explained by the "space-charge depletion layer model" [10]. According to this model, the 'electrical grain boundary' consists of a grain-boundary core with an enhanced oxygen vacancy concentration and two adjacent space-charge layers where oxygen vacancies are depleted, blocking the transport of oxide ions. The depletion of oxygen vacancies in the space-charge layers is due to the segregation of the dopant cation which has been proposed to be a grain size-dependent effect: segregation occurs over a larger grain-boundary area as the grain size decreases. Segregation of the dopant cation has also been observed in YSZ and ceria-based electrolytes [10,28,29].

In this work, we have investigated the transport properties of fine-grained ScSZ ceramics with low Si content. We chose a nominal composition of ZrO_2–6 mol% Sc_2O_3 in order to avoid the presence of the low-conductivity monoclinic and rhombohedral phases, which are usually detected in materials with lower and higher Sc_2O_3 contents, respectively. Taking into account that the presence of the β-phase strongly depends on the compositional homogeneity and the thermal history of the material, we decided to analyze samples with relatively low Sc_2O_3 content. The electrochemical impedance spectroscopy study presented here demonstrates that both the volume fraction of grain boundaries and the specific grain-boundary conductivity are significantly enhanced with decreasing average grain size, resulting in a higher total ionic conductivity. To our knowledge, this interesting behavior of fine-grained ScSZ electrolytes has not been reported before and can be very important since it strongly suggests that nanostructured samples may exhibit even better properties.

2. Experimental

ZrO_2–6 mol% Sc_2O_3 (nominal composition) nanopowders were synthesized by a nitrate-lysine gel-combustion route [30] using the following high-purity, raw compounds: $ZrO(NO_3)_2{\cdot}XH_2O$ ($X \approx 2$; Alpha Aesar; 99.995%; Si content <1 ppm) and $Sc(NO_3)_3{\cdot}4H_2O$ (Stanford Materials; 99.99%; Si content: 12 ppm). Dense ScSZ samples were prepared by uniaxial pressing and sintering in air under three different conditions: (i) pressing at 300 MPa and sintering in air at 1600 °C for 4 h; (ii) pressing at 300 MPa and sintering at 1350 °C for 2 h; (iii) pressing at 600 MPa and sintering at 1350 °C for 2 h.

X-ray fluorescence (XRF) analysis was performed to determine Sc_2O_3 and impurity contents in the as-synthesized powders and in the sintered specimens, using a PW4110 Venus 200 MiniLab X-ray spectrometer, with a Cr target transmission X-ray tube and a LiF(2 0 0) analyzer. The Si content of the as-synthesized nanopowders was also determined by Inductively Coupled Plasma-Optical Emission Spectroscopy (ICP-OES, Optima 2000 DV, PerkinElmer). For this analysis, the nanopowders were dissolved in H_2SO_4 and H_2O (H_2SO_4:H_2O = 5:3) by microwave digestion. The ICP-OES technique was not employed to analyze the dense ceramics because it was not possible to dissolve them in similar conditions, even after a milling step.

The crystalline phases of dense ScSZ ceramics were identified by X-ray diffraction (XRD, Philips PW 3710). Their density was determined from their mass and dimensions. Their microstructure was observed by scanning electron microscopy (SEM, Philips 515 microscope). During these observations, energy-dispersive spectroscopy (EDS) analyses were performed using an EDAX 9900 analyzer in order to detect the presence of impurities.

The ionic conductivity was measured by two-probe electrochemical impedance spectroscopy (EIS) from 200 to 600 °C in air using a Solartron 1255 frequency response analyzer and an EG&G Princeton Applied Research 273A potentiostat, in the frequency range of 0.1–10^5 Hz. For these measurements, Ag electrodes were applied on both sides of the ScSZ pellets by painting with a commercial paste and firing at 700 °C for 1 h.

3. Results and discussion

The Sc_2O_3 content of both as-synthesized nanopowders and dense ceramics, as determined by XRF, was 6.5 ± 0.6 mol% Sc_2O_3. In both cases, the Si content was lower than the limit of detection, which was found to be 1000 ppm. No other impurities were detected. According to ICP-OES analysis, the Si content in the as-synthesized nanopowders was 131 ± 10 ppm. The source of this small amount of Si was probably the Pyrex vessel used for the synthesis of the nanopowders. Since we did not use Si-containing materials for the preparation of the dense ceramics, it can be safely assumed that their Si content is similar to that of the nanopowders.

All ScSZ ceramics exhibited a mixture of tetragonal and cubic phases, as expected for this composition [31]. From Rietveld refinements of XRD data, it was possible to determine the rate of these phases, which were about 50:50 wt.% for all samples. The theoretical (crystallographic) density of this mixture of phases can be estimated as 5.77 g cm^{-3}, assuming theoretical densities of the tetragonal and cubic phases of 5.89 g cm^{-3} and 5.65 g cm^{-3}, respectively (Inorganic Crystal Structure Database, ICSD, cards # 86700 and 86707, based on data reported by Fujimori et al. [32]). As shown in Fig. 1, no traces of the monoclinic and rhombohedral phases were detected, since their most intense Bragg peaks (at 2θ angles

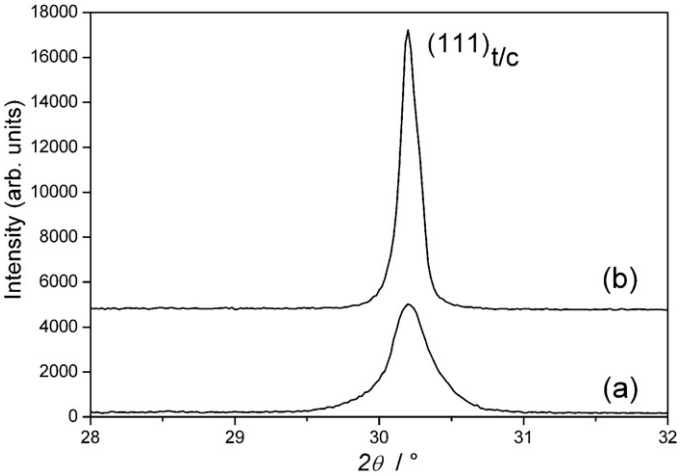

Fig. 1. Low-angle region of XRD patterns corresponding to ScSZ ceramics prepared by pressing at 600 MPa and sintering at 1350 °C (a) and by pressing at 300 MPa and sintering at 1600 °C (b). XRD data for samples prepared by pressing at 300 MPa and sintering at 1350 °C were similar to (a).

at the right or the left of the $(1\,1\,1)_{t/c}$ peak) were not observed. This is very important considering that these phases have very poor electrical properties and, therefore, their presence even in a small volume fraction may strongly affect the electrical properties of ScSZ ceramics.

Fig. 2 shows SEM micrographs of ScSZ samples studied in this work. Those sintered at 1350 °C exhibited relative densities of 94–96% and were formed by very small grains with uniform size, with average grain sizes in the range of 0.45–0.50 μm. Samples prepared with lower compaction pressure exhibited higher porosity. Those sintered at 1600 °C, with relative densities of 97%, exhibited a different microstructure, with much larger average grains (average grain size of 2.2 μm) and two typical sizes. Since it is well known that the grain growth kinetics of the tetragonal phase is significantly slower than that of the cubic phase [33], the smaller grains (with typical sizes of 1–1.5 μm) can be associated with the tetragonal phase and the larger ones (in the range of 3–4 μm) with the cubic phase. We did not find any glassy regions, usually observed when Si impurities form a SiO_2 phase. In addition, no impurities were detected by EDS.

Table 1 reports the total ionic conductivity at 600 °C (the highest temperature analyzed in this work) for all our ScSZ ceramics. The total ionic conductivity of the sample sintered at 1600 °C is comparable to those reported in the literature for materials with similar compositions [34–36]. Interestingly, samples sintered at 1350 °C exhibited higher ionic conductivity at high temperatures, as it can be noticed in the Arrhenius plots shown in Fig. 3.

The activation energies determined for the whole temperature range analyzed in this work, 200–600 °C, are reported in Table 1. Samples sintered at 1350 °C exhibited a higher activation energy (see the higher slope in the Arrhenius plots displayed in Fig. 3), probably due to the strong influence of the grain-boundary ionic transport in materials with small average grain size. In fact, Xu et al. reported that the activation energy of this process increases with decreasing grain size [25], in agreement with our results.

Table 1
Total ionic conductivity (σ) at 600 °C and activation energy in the whole temperature range 200–600 °C (E_a) of all ScSZ ceramics studied in this work (P = compaction pressure; T_s = sintering temperature). Numbers in parentheses indicate the error in the last significant digit.

Sample	σ (10^{-3} S cm^{-1})	E_a (eV)
P = 300 MPa; T_s = 1600 °C	6.1 (1)	1.21 (1)
P = 300 MPa; T_s = 1350 °C	8.6 (1)	1.27 (2)
P = 600 MPa; T_s = 1350 °C	9.8 (1)	1.28 (2)

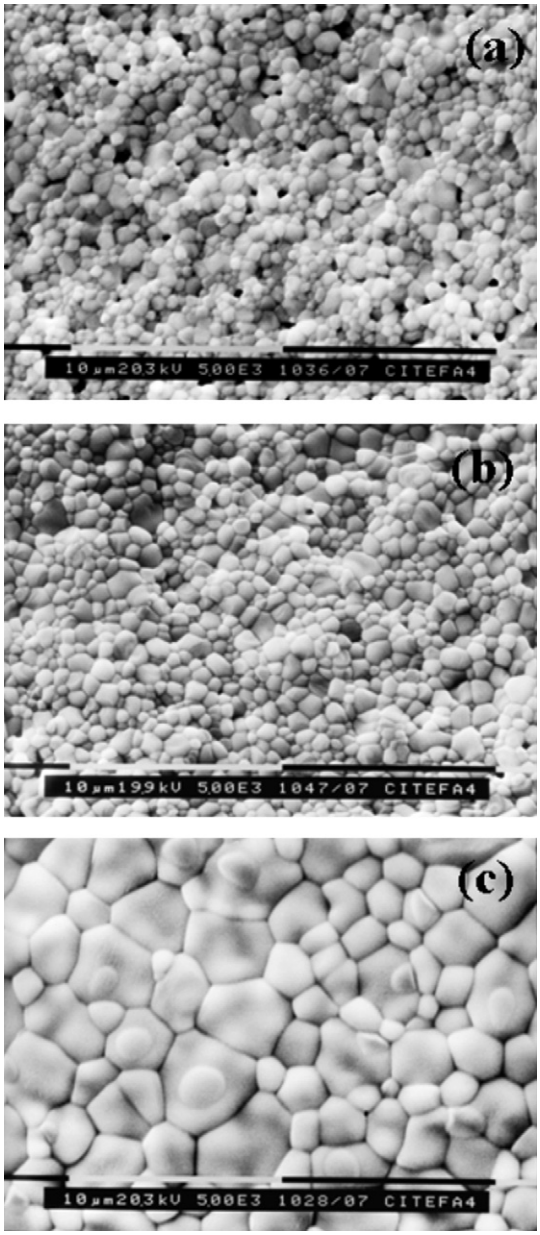

Fig. 2. SEM micrographs of ScSZ samples evaluated in this work, taken at 5000×. In all cases, the white line corresponds to 10 μm. (a) Pressed at 300 MPa and sintered in air at 1350 °C for 2 h; (b) pressed at 600 MPa and sintered at 1350 °C for 2 h; (c) pressed at 300 MPa and sintered at 1600 °C for 4 h.

Fig. 4 displays the Nyquist plots of ScSZ ceramics prepared under the different conditions studied in this work, measured at 225 °C. This temperature was chosen in order to have the complete arcs for both bulk and grain-boundary transport processes. It can be observed that the samples sintered at 1350 °C exhibited a smaller grain-boundary resistivity/bulk resistivity ratio, in spite of the larger number of grain boundaries and the smaller relative density. Besides, the bulk and grain-boundary arcs are more overlapped in the case of ceramics with small average grain size, indicating that the characteristic frequencies of both processes are closer. The analysis of the imaginary part of the impedance, shown in Fig. 5, confirms this behavior: two characteristic frequencies are clearly observed for the ceramic sintered at 1600 °C, while a strong overlap can be observed in the case of the samples sintered at 1350 °C.

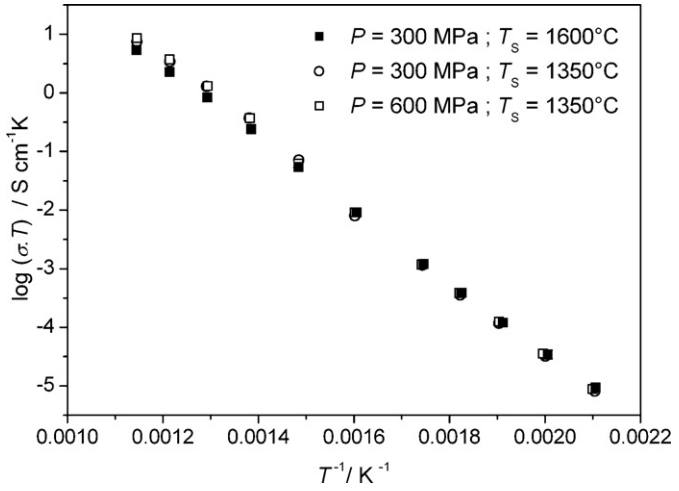

Fig. 3. Arrhenius plots (of total electrical conductivity) for ScSZ ceramics prepared under the different compaction pressures (P) and sintering temperatures (T_s) evaluated in this work.

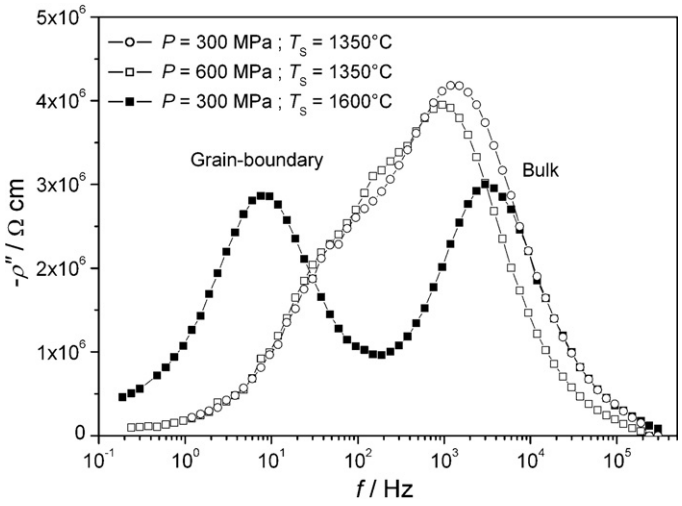

Fig. 5. Imaginary part of the impedance, $-\rho''$, as a function of frequency, measured at 225 °C, for all ScSZ samples analyzed in this work.

The increase in the characteristic frequency of the grain-boundary transport process and the enhancement of the total ionic conductivity found for samples with small average grain size point out that these fine-grained materials exhibit a different behavior than that of conventional microcrystalline ones. In order to achieve a better understanding of these results we will analyze our data in more detail.

EIS data shown in Fig. 4 were fitted by an equivalent circuit consisting of two parallel circuits of a resistance and a constant phase element (CPE, $Z_{CPE} = 1/Q(j\omega)^n$) in series. The 'true' capacitance can be calculated from the parameters Q and n using the equation [37]:

$$C = Q^{1/n}\rho^{(1-n)/n} \tag{1}$$

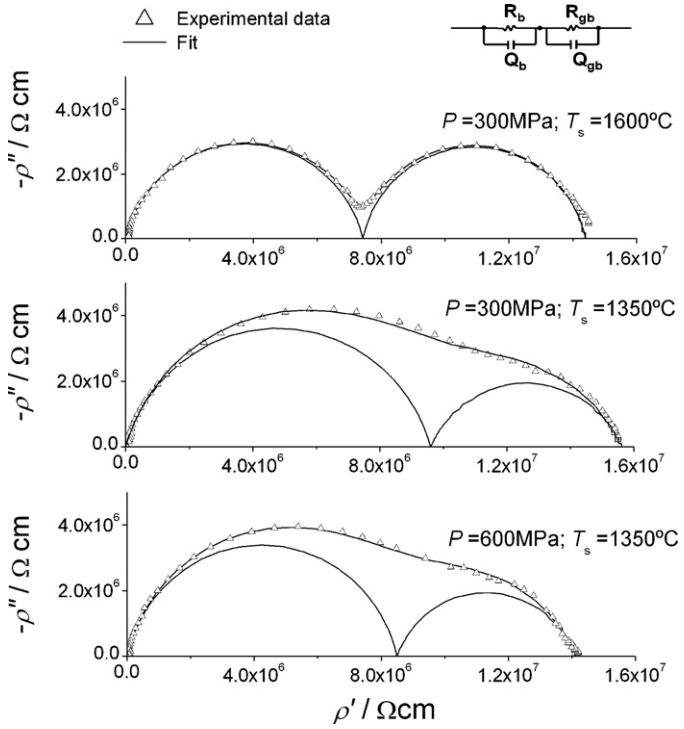

Fig. 4. Nyquist plots, measured at 225 °C, for all ScSZ samples studied in this work. The equivalent circuits used for fits are shown at the top of the figure. See text for details.

From the results of bulk and grain-boundary resistivities (ρ_b and ρ_{gb}, respectively) and the bulk and grain-boundary capacitances (C_b and C_{gb}, respectively), several parameters related to both transport processes can be determined as follows [10]:

$$f_c^i = \frac{(\rho_i Q_i)^{-1/n_i}}{2\pi} = \frac{1}{2\pi\rho_i C_i} \quad (i = b; gb) \tag{2}$$

$$\frac{\delta}{D} = \frac{\varepsilon_{gb}C_b}{\varepsilon_b C_{gb}} \approx \frac{C_b}{C_{gb}} \tag{3}$$

$$x = \frac{3D^2\delta}{D^3 + 3D^2\delta} \approx \frac{3\delta}{D} \tag{4}$$

$$\sigma'_{gb} = \frac{\sigma_{gb}\delta}{D} \approx \frac{\sigma_{gb}C_b}{C_{gb}} \tag{5}$$

$$\frac{\sigma_b}{\sigma'_{gb}} \approx \frac{\sigma_b C_{gb}}{\sigma_{gb}C_b} = \frac{f_c^b}{f_c^{gb}} \tag{6}$$

where f_c^i is the characteristic frequency of the process, ε is the dielectric constant, x is the volume fraction of grain boundaries and the subscripts or superscripts b and gb indicate bulk and grain-boundary transport processes, respectively. In Eq. (3), it has been assumed that $\varepsilon_{gb} \approx \varepsilon_b$, which is considered a reasonable approximation in ZrO_2-based materials [10]. The results of this analysis are summarized in Table 2.

The results of EIS analysis for the ScSZ sample sintered at 1600 °C ($D = 2.2$ μm) are in agreement with those known for conventional microcrystalline materials, since σ_b is more than two orders of magnitude higher than σ'_{gb}, $\delta \approx 5$ nm is typical for ZrO_2- or CeO_2-based materials [10] and x is very small. In this case, grain boundaries only block ionic transport and its parallel component is negligible. On the other hand, for samples sintered at 1350 °C ($D \approx 0.50$ μm), the σ_b/σ'_{gb} ratio decreases by a factor of 20, showing that σ'_{gb} increases dramatically, and x becomes significant. Since bulk transport is still much faster than grain-boundary transport, the parallel grain-boundary conductivity is not high enough to reach very high total ionic conductivities. However, the increase of σ'_{gb} is important since it gives rise to higher total ionic conductivity at high temperatures for samples with small D (see Table 1). Taking into account this important result, the present work indicates that high-purity nanostructured ScSZ ceramics deserve intense investigation since the grain-boundary diffusivity may be enhanced by orders of magnitude in comparison to conventional microcrystalline materials.

Table 2
Results of EIS analysis for ScSZ samples prepared under different conditions (P = compaction pressure; T_s = sintering temperature; D = average grain size). The subscripts or superscripts "b" and "gb" indicate bulk and grain-boundary transport processes, respectively. Numbers in parentheses indicate the error in the last significant digit.

	P = 300 MPa T_s = 1600 °C D = 2.2 μm	P = 300 MPa T_s = 1350 °C D = 0.45 μm	P = 600 MPa T_s = 1350 °C D = 0.50 μm
ρ_b (Ω cm)	7.43 (2) × 10^6	9.6 (5) × 10^6	8.5 (3) × 10^6
Q_b (F cm^{-1})	2.82 (5) × 10^{-11}	4.7 (2) × 10^{-11}	5.4 (1) × 10^{-11}
n_b	0.852 (2)	0.821 (7)	0.857 (4)
C_b (F cm^{-1})	6.5 (1) × 10^{-12}	8.8 (5) × 10^{-12}	1.50 (4) × 10^{-11}
f_c^b (Hz)	3.30 (6) × 10^3	1.9 (2) × 10^3	1.25 (7) × 10^3
ρ_{gb} (Ω cm)	6.97 (8) × 10^6	6.0 (4) × 10^6	5.6 (3) × 10^6
Q_{gb} (F cm^{-1})	4.8 (2) × 10^{-9}	1.7 (1) × 10^{-9}	1.7 (1) × 10^{-9}
n_{gb}	0.870 (8)	0.73 (4)	0.77 (3)
C_{gb} (F cm^{-1})	2.9 (1) × 10^{-9}	3.0 (2) × 10^{-10}	4.1 (3) × 10^{-10}
f_c^{gb} (Hz)	7.9 (4)	88 (9)	69 (8)
δ (nm)	4.9 (5)	13 (2)	18 (2)
x (%)	0.67 (7)	8 (1)	10 (1)
σ_b/σ'_{gb}	4.2 (2) × 10^2	22 (4)	18 (3)

The results of the present work show that the grain-boundary diffusivity of oxide ions in ScSZ ceramics increases with decreasing grain size, in qualitative agreement with Xu et al. [25]. As has been mentioned above, these authors reported a marked increase in σ'_{gb} with decreasing grain size in samples prepared by a hydrothermal process in the presence of urea. Unfortunately, the authors did not report the Si content of their samples, but they suggested that their results can be explained by SiO_2 segregation. In our case, we are dealing with materials with low Si content and, therefore, other mechanisms must be considered, such as the space-charge depletion layer model. In this context, our results can be understood assuming that Sc segregation is enhanced with decreasing grain size, thus causing an increase in both δ and the oxygen vacancy concentration and also a decrease in the σ_b/σ'_{gb} ratio [10,38]. The relatively large values of δ found in the present work can be related to this grain-size-dependent grain-boundary segregation of the dopant cation, which is expected to become more important in fine-grained or nanocrystalline materials [10,38]. Further investigation is needed to fully address this issue.

4. Conclusions

We have studied the electrical properties of fine-grained ScSZ ceramics with low concentration of Si impurities that were prepared under different conditions. EIS analysis showed that both the volume fraction of grain boundaries and the specific grain-boundary conductivity are significantly enhanced with decreasing grain size. As a consequence, ScSZ ceramics of small average grain size (0.45–0.50 μm) exhibited higher total ionic conductivity than microcrystalline samples. This can be explained in the context of the space-charge depletion layer model if grain size-dependent segregation of Sc takes place, occurring in a larger region as the grain size decreases.

In view of our results, it is clear that the study of the ionic transport properties of dense ScSZ nanoceramics with a smaller grain size deserves great attention, since they may exhibit much better properties than conventional microcrystalline ceramics.

Acknowledgements

The present work was supported by Agencia Nacional de Promoción Científica y Tecnológica (Argentina, PICT 2005 No. 38309 and PICT 2007 No. 1152) and CONICET (PIP No. 6559). The authors thank N. Calviño, M. Molina and R. Tarulla (Departamento de Química Aplicada, CITEFA) for ICP-OES analysis and useful discussions, M. Ortiz (CAC, CNEA) for her help in XRF study and M. Moraga and Elsevier Language Editing Services for English revision. P.M. Abdala thanks CONICET and Fundación YPF for her doctoral fellowship.

References

[1] H.L. Tuller, Solid State Ionics 131 (2000) 143.
[2] A. Cheikh, A. Madani, A. Touati, H. Boussetta, C. Monty, J. Eur. Ceram. Soc. 21 (2001) 1837.
[3] C. Monty, Ionics 8 (2002) 461.
[4] P. Heitjans, S. Indris, J. Phys.: Condens. Matter 15 (2003) R1257.
[5] A.V. Chadwick, Diff. Fund. 2 (2005) 44.
[6] M.G. Bellino, D.G. Lamas, N.E. Walsöe de Reca, Adv. Funct. Mater. 16 (2006) 107.
[7] M.G. Bellino, D.G. Lamas, N.E. Walsöe de Reca, Adv. Mater. 18 (2006) 3005.
[8] M. Aoki, Y.M. Chiang, I. Kosacki, L.J.R. Lee, H.L. Tuller, Y.P. Liu, J. Am. Ceram. Soc. 79 (1996) 1169.
[9] X. Guo, J. Maier, J. Electrochem. Soc. 148 (2001) E121.
[10] X. Guo, R. Waser, Prog. Mater. Sci. 51 (2006) 151.
[11] I. Kosacki, T. Suzuki, V. Petrovsky, H.U. Anderson, Solid State Ionics 136–137 (2000) 1225.
[12] T. Suzuki, I. Kosacki, H.U. Anderson, Solid State Ionics 151 (2002) 111.
[13] S. Jiang, W.A. Schulze, V.R.W. Amarakoon, G.C. Stangle, J. Mater. Res. 12 (1997) 2374.
[14] Y.M. Chiang, E.B. Lavik, D.A. Blom, Nanostruct. Mater. 9 (1997) 633.
[15] V.V. Kharton, F.M.B. Marques, A. Atkinson, Solid State Ionics 174 (2004) 135.
[16] S.P.S. Badwal, F.T. Ciacchi, D. Milosevic, Solid State Ionics 136–137 (2000) 91.
[17] T.I. Politova, J.T.S. Irvine, Solid State Ionics 168 (2004) 153.
[18] Z. Wang, M. Cheng, Z. Bi, Y. Dong, H. Zhang, J. Zhang, Z. Feng, C. Li, Mater. Lett. 59 (2005) 2579.
[19] M.A. Laguna-Bercero, S.J. Skinner, J.A. Kilner, J. Power Source 192 (2009) 126.
[20] E.S. Raj, A. Atkinson, J.A. Kilner, Solid State Ionics 180 (2009) 952.
[21] Z. Lei, Q. Zhu, Solid State Ionics 176 (2005) 2791.
[22] M. Okamoto, Y. Akimune, K. Furuya, M. Hatano, M. Yamanaka, M. Uchiyama, Solid State Ionics 176 (2005) 675.
[23] P.M. Abdala, A.F. Craievich, M.C.A. Fantini, M.L.A. Temperini, D.G. Lamas, J. Phys. Chem. C 113 (2009) 18661.
[24] K. Biswas, Ceram. Int. 35 (2009) 2047.
[25] G. Xu, Y.-W. Zhang, C.-S. Liao, C.-H. Yan, Solid State Ionics 166 (2004) 391.
[26] M.J. Verkerk, B.J. Middelhuis, A.J. Burggraaf, Solid State Ionics 6 (1982) 159.
[27] X. Guo, Z. Zhang, Acta Mater. 51 (2003) 2539.
[28] Y. Ikuhara, P. Thavorniti, T. Sakuma, Acta Mater. 45 (1997) 5275.
[29] Y. Lei, Y. Ito, N.D. Browning, T.J. Mazanec, J. Am. Ceram. Soc. 85 (2002) 2359.
[30] P.M. Abdala, R. Kempf, D.G. Lamas, ECS Trans.: Solid Oxide Fuel Cells 7 (2007) 2197.
[31] M. Yashima, M. Kakihana, M. Yoshimura, Solid State Ionics 86–88 (1996) 1131.
[32] H. Fujimori, M. Yashima, M. Kakihana, M. Yoshimura, J. Am. Ceram. Soc. 81 (1998) 2885.
[33] W.E. Lee, W.M. Rainforth, Ceramic Microstructures: Property Control by Processing, Chapman & Hall, London, 1994, p. 317.
[34] S.P.S. Badwal, Solid State Ionics 52 (1992) 23.
[35] Y. Arachi, H. Sakai, O. Yamamoto, Y. Takeda, N. Imanishai, Solid State Ionics 121 (1999) 133.
[36] I. Kosacki, H.U. Anderson, Y. Mizutani, K. Ukai, Solid State Ionics 152–153 (2002) 431.
[37] E. Chinarro, J.R. Jurado, F.M. Figueiredo, J.R. Frade, Solid State Ionics 160 (2003) 161.
[38] X. Guo, Comput. Mater. Sci. 20 (2001) 168.